Application of an Avalanche Photodiode in Ultrafast X-radiography

S.-K. Cheong,[1] J. Liu,[1] C.F. Powell,[2] J. Wang[1]
[1]Advanced Photon Source (APS) and
[2]Center for Transportation Research, Argonne National Laboratory, Argonne, IL, U.S.A.

Introduction

Avalanche photodiodes (APDs) have been used in synchrotron-radiation-based applications and have led to numerous advances in nuclear resonant scattering [1, 2] and time-resolved studies [3]. For most synchrotron x-ray applications, APDs are normally operated in a photon-counting mode. When a pulsed x-ray source such as a synchrotron is used, detectors in the photon-counting mode are saturated well below 1 incident photon per synchrotron bunch. To overcome this difficulty, APDs has been employed in continuous wave (cw) mode for an application of ultrafast x-radiography [3, 4].

Synchrotron radiation sources produce bursts of radiation as a result of the electron bunch structure in the storage ring. Since the interval between bunches (approximately 150 nanoseconds [ns]) is longer than the dead time of the APD, it is possible to perform time-resolved experiments on a time scale of nanoseconds by taking advantage of the pulsed time structure in the storage ring. The APDs used in our measurements have a temporal time resolution of 2 ns, which is much longer than the synchrotron bunch width (50-100 picoseconds [ps]) but much shorter than the bunch intervals. Although these detectors are not one of the fastest detectors, their time resolution is good enough to perform the microsecond (μs) time-resolved x-radiography.

In the application of the fuel spray x-radiography using x-ray transmission, we recorded the response of the APD detector for a time span of 1 ms for a spray with a typical duration of 400 μs. It requires one million data points to obtain 1 ns of data resolution, which demands a huge amount of computer readout time. In some cases, a time window for measurements needs to cover a wider data range for longer spray durations. Therefore, there is a limit for increasing the data resolution in this type of measurement, which hinders the acquisition of a good pulse shape. Without a good pulse shape, it becomes difficult to determine the amplitude of the pulse. This drives us to develop a fitting and an integration method during data processing, as discussed below.

In this work, we investigated a $5 \times 5\text{-mm}^2$ APD designed by EG&G Optoelectronics, which has been used as a timing detector in ultrafast x-radiography. We studied its linearity and signal-to-noise ratio (S/N) through data treatments as well as its time resolution with several amplification circuit configurations.

Methods and Materials

The detector measurements were performed at bending magnet beamline station 1-BM-C at the APS. In single-bunch mode, the synchrotron produced 23 x-ray pulses with a maximum current of ~4.5 mA and a spacing of 153 ns between pulses followed by a 306-ns gap. The radiation produced by a bending magnet was monochromatized to 6.0 keV by using a double-crystal monochromator. The APD signal output was digitized by a 500-MHz oscilloscope (LeCroy WavePro 940). Figure 1 shows a schematic of the electronic configuration used in this work.

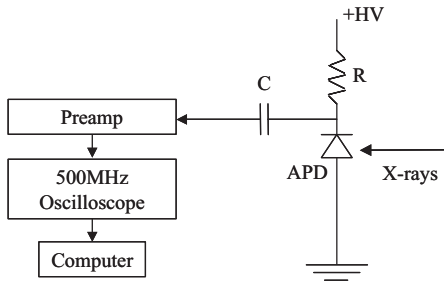

FIG 1. Schematic of the electronic configuration. HV = 280 V, C = 220 pF, and R = 1 MΩ.

The main electronic ingredient used in this work is an ac-coupled amplifier with a gain of 40 dB at 100 MHz. The rise and fall times are about 2.5 ns, giving a total FWHM of 4.0 ns. Replacing the amplifier with a high-bandwidth one (a gain of 26 dB at 12.5 GHz) improves the time response by 8% (about 2.3 ns of the rise/fall times) and provides a poor pulse shape with ringing due to the reflection with the other components, revealing that time resolution is limited by the APD, the slowest component in this configuration. Although a dc-coupled configuration provides a faster response (1.7 ns for the rise time), it has a signal that is 3 times lower than that of the ac-coupled amplifier. Unlike the time resolution in other fast counting measurements, the time resolution of the detector is less important than its linearity and S/N for achieving a quantitative result in the x-radiography of the fuel spray.

Since there are 23 bunches of the single-bunch mode at the APS within one cycle (frequency of 272 kHz), each x-ray pulse arrives at a frequency of 6.5 MHz. We recorded the response of the APD detector for a

time span of 100 μs containing 27 cycles (27 × 23 = 621 pulses). The intensity impinging on the detector was varied by altering the throughput of the monochromator. This was accomplished by varying the angle of the second crystal with respect to the first crystal. A scintillation counter masked by several attenuators with known attenuation factors at this photon energy was used to correlate the absolute number of photons with an ion chamber in front of the APD detector.

Results

In the cw mode, shifts of baseline of the signal were observed as a function of the beam intensity. This fluctuation alters the amplitude of the pulse. To remove the unwanted signals between pulses (mainly from background radiations), which worsen S/N if included, data were prepared by gating the pulse of the APD signal (typically picking data points between 5 ns ahead of the peak and 10 ns behind the peak). Figure 2(a) shows the digitized signal from the detector for a time span of 10 μs. Symbols in Fig. 2(b) show the gated pulses as described above. As can be seen in Fig. 2(b), the first peak of the pulse is the response of detector to the x-ray burst, and the second peak is due to reflection from interfaces of electronics and cables.

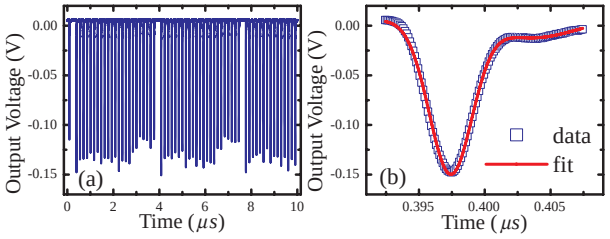

FIG. 2. (a) Digitized signal from the APD detector for a time span of 10 μs. (b) Symbols show the gated pulse for data processing. Solid line represents fit with two Gaussian functions.

Data analysis was done by using two different methods. One was by fitting two Gaussian functions to the each gated pulse. A typical fit to the gated pulse is shown as a solid line in Fig. 2(b). The Gaussian function G(t) used was:

$$G(t) = A_1 \exp\left[-\frac{(t-a_1)^2}{2w_1^2}\right] + A_2 \exp\left[-\frac{(t-a_2)^2}{2w_2^2}\right] + A_0. \quad (1)$$

The background (A_0) was held at an average of the data values within 30 ns ahead of each pulse to correct the changes in the amplitude due to the baseline fluctuation, while the other remaining variable parameters (A_1, A_2, a_1, a_2, w_1, and w_2) were floated. By using average values from the best fits to 23 pulses of the cycle, the ratio between two amplitudes (A_1/A_2), the difference between centers of two peaks (a_2-a_1), and the widths (w_1 and w_2) can be fixed. Furthermore, a_1 of each pulse can be directly determined from the raw data because of the precise timing structure of the synchrotron pulse. Thus with only one adjustable parameter (A_1) and with the other parameters held at their fixed values, we were able to fit the Gaussian function in Eq. (1) to every pulse in a given time span without trapping at local minima of least squares fitting.

The other method used in the analysis is integration of the gated pulse, which is proportional to the accumulated charge inside the detector. This is done by adding the differences between data values and background. The integrations are summed for a complete cycle (3.68 μs), resulting in 27 data points for the time span of 100 μs. It turned out that the integration method is superior to the fitting method for most of cases, as discussed below.

The detector linearity was investigated by using both the fitting method and the integration method. Figures 3(a) and 3(b) show the output voltages (pulse heights) from the fit and the integrated area of the gated pulse as a function of the number of photons per pulse incident on the APD detector, respectively. As shown in Fig. 3(a), the pulse height is suppressed because of the detector saturation above 200 photons per pulse (10% deviation from dynamic region), which corresponds to 1.25 × 109 photons per second.

However, the integration of the gated pulse provides a wider dynamic range than the pulse height. Integration deviates from the linear region above approximately 500 photons per pulse (10% deviation from dynamic region). Figure 3(c) shows outputs normalized by dividing by maximum values of the fit (squares) and the integration (circles), respectively. When the pulse height is suppressed due to saturation, the pulse width becomes slightly wider. As a result, integration of the pulse compensates for the decrease in amplitude, resulting in better linearity over a wider dynamic range.

Improving S/N is desirable in most physical experiments to achieve reliable quantitative results.

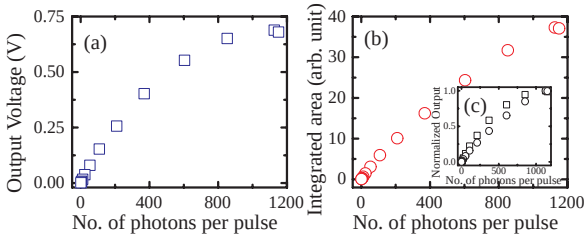

FIG. 3. (a) Output voltage (pulse height) from the fit as a function of number of photons per pulse. (b) Integrated area of the gated pulse as a function of number of photons per pulse. (c) Outputs normalized by dividing by the maximum values of the fit (squares) and the integration (circles), respectively.

Here we demonstrate how the S/N can be improved during processing of the same raw data.

The first step of the fitting method involves fitting two Gaussian functions to 23 pulses of the first cycle with six variables being adjustable. Next, fitting G(t) to all 27 × 23 pulses is followed with one variable being adjustable and the other variables being held at fixed values, as discussed above. The S/N obtained is described in Eq. (2):

$$(S/N)_i = \left(\frac{Amp_{av}}{Amp_{std}}\right)_i, \quad S/N = \frac{\sum_{i=1}^{23}(S/N)_i}{23}, \qquad (2)$$

where Amp_{av} and Amp_{std} represent an average amplitude of i^{th} pulse of each cycle and its standard deviation, respectively. In the integration method, S/N was determined by an average value for all 27 cycles divided by its standard deviation. S/N as a function of the number of shots for average and S/N as a function of digitizing resolution are shown in Figs. 4(a) and 4(b), respectively. The beam intensity was optimized for about 300 photons per pulse. In both cases, the S/N from using the integration method is about five times higher than that from using the fitting method. By using the integration method, we were able to achieve a S/N of 1000 with 200 shots of 300 photons per pulse.

Performing the x-radiography of the fuel spray consists of measuring the x-ray transmission with the

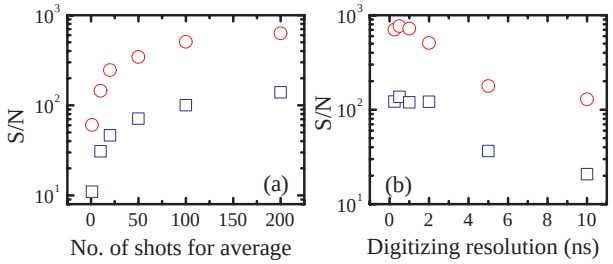

Fig. 4. (a) S/N as a function of number of shots for average. (c) S/N as a function of digitizing resolution. Squares and circles represent S/N from the fit and the integration, respectively.

APD as a point detector and translating an injection chamber vertically and horizontally with respect to the x-ray beam with micrometer resolution, which allows the beam to prove various positions within the spray fume. Figure 5 shows snapshots of the time evolution of diesel fuel sprays measured by x-radiography at different times after injection began.

In this measurement, about 100 to 200 photons per pulse reach the detector after passing through the fuel injection chamber filled with pressurized ambient gases. With this number of photons, we were able to achieve 350 to 500 S/N from the integration by averaging the results of 50 to 100 measurements.

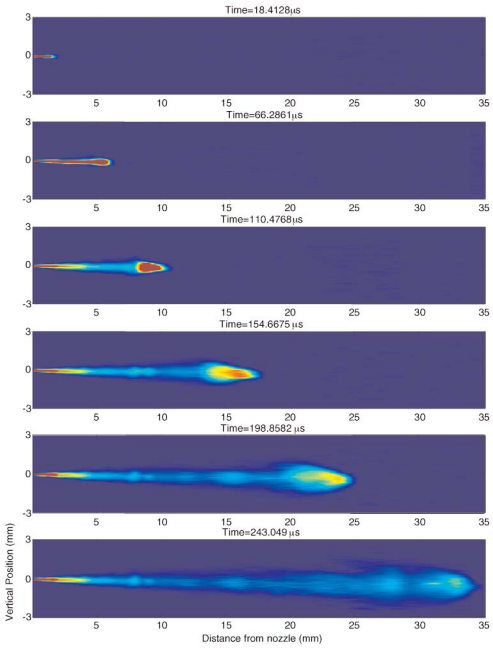

Fig. 5. Snapshots of time-evolution of diesel fuel sprays measured by x-radiography at different times after start of injection.

Discussion

We demonstrated that the APD has been successfully used in the cw mode to perform the microsecond-time-resolving x-radiography of the fuel spray. In the cw mode, the integration of the gated pulse provides better linearity and S/N than the fitting to the height of the pulse. It encourages us to develop an APD array detector with smaller elements to cover a larger area in order to reduce measurement time and achieve finer spatial resolution.

Acknowledgments

This work was performed at the 1-BM-C beamline station of the APS. Use of the APS was supported by the U.S. Department of Energy (DOE), Office of Science, Office of Basic Energy Sciences, under Contract No. W-31-109-ENG-38. This work was supported by the DOE Office of Transportation Technologies, FreedomCAR and Vehicle Technology Program.

References

[1] S. Kishimoto, N. Ishizawa, and T.P. Vaalsta, Rev. Sci. Instrum. **69**, 384-391 (1998).

[2] A.Q.R. Baron, R. Rüffer, and J. Metge, Nucl. Intrum. Methods A **400**, 124-132 (1997).

[3] A.G. MacPhee, M.W. Tate, C.F. Powell, Y. Yue, M.J. Renzi, A. Ercan, S. Narayanan, E. Fontes, J. Walther, J. Schaller, S.M. Gruner, and J. Wang, Science **295**, 1261-1263 (2002).

[4] C.F. Powell, Y. Yue, R. Poola, and J. Wang, J. Synchrotron Radiat. **7**, 356-360 (2000).